

1 **Modeling and Simulation of Creep Response of Sorghum Stems: Towards an**
2 **Understanding of Stem Geometrical and Material Variations**

4 Omid Zargar, Matt Pharr, and Anastasia Muliana
5 Department of Mechanical Engineering, Texas A&M University

7 **Abstract**

8 Sorghum [*Sorghum bicolor (L.)*] is a tropical grass that often suffers from structural failure
9 (lodging) when subjected to wind, rain, and hail. During lodging, excessive lateral deflection occurs, which
10 inherently correlates with the biomechanical properties of the stem. As such, a fundamental understanding
11 of sorghum's biomechanical behavior is required to mitigate its propensity for lodging. Herein, we perform
12 creep tests to characterize the mechanical behavior of Della genotype sorghum stems and their constituents,
13 i.e., their rind and pith. This study also examines the influence of various testing geometries and boundary
14 conditions on mechanical property characterization. We determine that small geometric irregularities
15 typical of sorghum stems (e.g., from straight circular cylinders) do not affect their mechanical response in
16 an overall engineering strain sense. However, these typical geometric irregularities do lead to nonuniform
17 (localized) stresses and strains, thereby influencing the quantification of certain properties during
18 mechanical testing. We also implement a viscoelastic constitutive model to describe the creep responses of
19 the individual constituents (rind and pith), as to predict the overall biomechanical response of the stems.
20 We find that even though the rind carries most of the load in the stem and itself does not show a significant
21 time-dependent response, an overall time-dependent response of the stem still occurs, arising from
22 viscoelastic effects in the pith.

23 **Keywords:** Sorghum; Stem lodging; Biomechanical response; Creep; Viscoelasticity; Specimen morphologies

1 **1. Introduction**

2 Cereal crops (e.g., sorghum, corn, rice, etc.) are susceptible to lodging when exposed to dynamic
3 forces from wind, rain, hail, etc. Lodging is associated with excessive lateral displacements (bending) of
4 plant stems which disrupt their growth and development, and can further lead to stem breaking (stem
5 lodging) and/or anchorage failure (root lodging). Dwarf varieties were widely used during the Green
6 Revolution era to minimize lodging from mechanical forces, which significantly improved cereal crop
7 yields. However, with global climate changes and an increase in crop yields, the dwarf varieties have
8 become less effective, and the frequency of lodging has increased (Berry et al., 2004; Hirano, Ordonio, &
9 Matsuoka, 2017; Niu, Feng, Ding, & Li, 2016). In the past ten years, efforts in mitigating lodging in rice,
10 wheat, sorghum, and maize have shifted to the understanding of the biomechanics of stems with the
11 intention to develop new lodging-resistant variants (Berry et al., 2004; Hirano et al., 2017).

12 The biomechanical behavior of plants has been widely investigated, mainly regarding their elastic
13 properties, through experimentation (Gomez, Carvalho, Shi, Muliana, & Rooney, 2018; Gomez, Muliana,
14 & Rooney, 2018; Robertson, Julias, Lee, & Cook, 2017; Robertson, Smith, & Cook, 2015). However,
15 testing of these plants presents challenges in terms of proper characterization relative to standard
16 engineering materials. As an example, in standard uniaxial compression tests, a straight cylindrical
17 specimen is often used. However, plants grow with irregular shapes that deviate from simple geometries
18 (e.g., perfect straight cylindrical sections). To the best of our knowledge, no standardized tests exist
19 specifically for fresh (live) plant tissues, which are complex composite systems and often of small size. A
20 few standards have been reported for lumber and wood materials (ASTM-D4761, Standard test methods
21 for mechanical properties of lumber and wood-based structural material) but these standards are not always
22 applicable to soft plant tissues. The lack of specific standards leads to difficulties in extracting useful
23 comparable information from different sources in literature, particularly in tests on fresh plant stems, which
24 have large contents of water. In conducting tensile testing of fresh stems, gripping presents challenges as
25 slippage often occurs in the grip area; these effects are less problematic in the testing of dry hollow stems
26 (Wright et al., 2005; Zeng, Mooney, & Sturrock, 2015). During compression tests, misalignment between
27 the samples and fixtures (e.g., compression platens) will result in nonuniform stress distributions and even
28 buckling and/or rotating of the samples due to geometric variation in both the cross-sectional and
29 longitudinal directions. Using self-aligning compression platens can partially mitigate this issue (Al-Zube,
30 Robertson, Edwards, Sun, & Cook, 2017), but challenges remain in properly determining the material
31 properties from the raw load-displacement test outputs.

32 Most experimental studies have focused on determining elastic properties and failure behaviors
33 under bending, tension, and compression (Al-Zube et al., 2017; Gomez, Muliana, Niklas, & Rooney, 2017;

1 Kin & Shim, 2010; Lemloh et al., 2014; Robertson et al., 2015; Wright et al., 2005). However, plant tissues
2 (dry or wet) show viscoelastic responses and exhibit microstructural reconfigurations due to mechanical
3 loadings. Thus, further experimental investigation on creep/viscoelastic and permanent deformation is of
4 interest. To this end, researchers have used a dead weight on living plants (in vivo) or plants submerged in
5 water (in vitro) to conduct creep tests, in which custom-built extensometers equipped with linear
6 displacement transducers can measure elastic, viscoelastic, and plastic deformations (Alméras, Gril, &
7 Costes, 2002; Edelmann & Köhler, 1995; Ulrich Kutschera & Briggs, 1987, 1988; U Kutschera & Schopfer,
8 1986; Robertson et al., 2017; Suslov & Verbelen, 2006). Recently, Lee. et al. (Lee et al., 2020) have
9 conducted uniaxial compression tests on fresh sorghum stems. They have found that sweet sorghum stems
10 exhibit significant time-dependent mechanical responses, owing to both viscoelastic and poroelastic
11 behavior. These time-dependent responses have important ramifications in stem lodging under dynamic
12 forces of various frequencies (e.g., due to wind).

13 As plant stems comprise hierarchical structures with different microstructural morphologies and
14 constituent responses, geometric features, including cross-sectional shapes and dimensions, can affect the
15 stress distribution in the stems and cause early failure in some regions (D. U. Shah, T. P. Reynolds, & M.
16 H. Ramage, 2017a). Additionally, the mechanical properties of the individual pith and rind constituents
17 together produce the overall mechanical responses of the stem. Wirawan et. al. (Wirawan, Sapuan, Robiah,
18 & Khalina, 2011) have shown that the elastic and viscoelastic properties of sugarcane composites are
19 correlated with the fiber content of pith and rind. Robertson et al. (Robertson et al., 2017) and Stubbs et al.
20 (Stubbs, Baban, Robertson, Alzube, & Cook, 2018) have shown that rind tissues are load-bearing
21 components in terms of longitudinal stresses produced by bending in thin-walled plant stems. In another
22 work, Al. Zube. et al. (Al-Zube et al., 2017) have demonstrated that the contribution of the pith tissue within
23 maize stems affects the compressive modulus of the stems; moreover, the presence of the pith tissues
24 prevents the stems from buckling and hence contributes to the overall strength of the stems (Zuber, Colbert,
25 & Darrah, 1980). Likewise, understanding the influence of morpho-anatomical and biomechanical
26 properties of tissues and cell components on the overall plant behaviors often relies on modeling and
27 simulation. Cisse et al. (Cisse, Placet, Guicheret-Retel, Trivaudey, & Boubakar, 2015) modeled the tensile
28 creep tests of hemp fibers using an anisotropic constitutive model developed by (Boubakar, Vang,
29 Trivaudey, & Perreux, 2003) to capture the long-term viscoelastic behavior. The model is based on
30 rheological models, e.g., generalized Kelvin-Voigt and Maxwell models. They have revealed that single
31 hemp fibers show significant delayed and large permanent strain due to loading and unloading, respectively,
32 which originates from instantaneous and time-dependent mechanisms. Recently, Song and Muliana (Song
33 & Muliana, 2019) proposed a constitutive material model to capture the creep tensile behavior of plant
34 stems, considering microstructural changes in stems during loading. They have incorporated the effects of

1 microstructural changes of plant networks on overall macroscopic mechanical behaviors using a multiple
2 natural configuration method, which was formulated and successfully implemented to describe responses
3 of soft materials (De Tommasi, Puglisi, & Saccomandi, 2006; Yuan, Muliana, & Rajagopal, 2020).

4 In this study, we investigate the biomechanical responses of sorghum stems, particularly their
5 viscoelastic responses. There are currently no standardized testing methods for characterizing the
6 biomechanical properties of plant stems, as pointed out by (Shah et al., 2017); instead, testing methods
7 commonly used for engineering materials have been adopted for testing plant stems. Difficulties in testing
8 plant stems arise from variability and complexity of the geometrical shapes of the stems, unlike in
9 engineering materials where sample size and shape can be readily controlled. To aid in addressing this
10 issue, herein we investigate the effects of geometrical characteristics of plant stems, different material
11 properties of the constituents (pith and rind), and boundary conditions in the experimental tests on the
12 overall biomechanical behavior. Specifically, we examine the sorghum [*Sorghum bicolor (L.)*] Della
13 genotype, as grown in a greenhouse. We conduct experimental creep tests under uniaxial compression on
14 sorghum stems and pith, and tests under uniaxial tension on the rind and pith. We then perform finite
15 element (FE) simulations of sorghum stems to better understand the influence of the variabilities in
16 geometries and boundary conditions on the stems' mechanical response during experimental testing. This
17 "virtual testing" can aid in characterizing the properties of plant stems and their constituents through
18 mimicking real experiments. As such, we first evaluate the influence of stem cross-sectional and
19 longitudinal nonuniformities on the overall creep response. We then study the effects of different creep
20 responses of the individual constituents (rind and pith) on the overall behavior of the stems.

21

22 **2. Materials and Methods**

23 ***2.1. Plant material***

24 One group of sorghum cultivar Della was selected for tensile creep testing and another for
25 compression creep testing. They were planted in February and April 2019, respectively, in the Borlaug
26 Center greenhouse located at 30.6° N in College Station, TX. Plants were grown in 19 L pots containing a
27 fine sandy loam soil amended with 14-14-14 slow-release fertilizer. The greenhouse temperature was 26-
28 30 °C day/21-26 °C night, and the photoperiod was 14 h day/10 h night, with supplemental light provided
29 by high-pressure sodium lamps. Each group was harvested for mechanical testing at grain maturity,
30 approximately 13 weeks after planting.

31

32 ***2.2. Sample preparation***

1 Plants were harvested for mechanical testing by cutting the stems at the soil level. All sorghum
 2 samples were collected in the morning before temperatures increased (8-10 AM), as to minimize the amount
 3 of water lost through evapotranspiration. All tests were performed within 6 hours after cutting the internode
 4 from the plant. Internode numbers were counted based on the first elongated internode above the ground to
 5 the last internode below the peduncle. For uniaxial tensile tests, the pith and rind specimens were cut into
 6 thin plate samples; while for the uniaxial compression tests the pith and the stem were cut into cylindrical
 7 shapes. The information regarding the type of testing, internode number, and sample sizes are categorized
 8 in **Table 1**.

9

10 **Table 1.** Testing type, internode number, and plant constituent anatomical properties

Type of Test	Internode Number	Plant Constituent	Dimensions (mm)			
			Diameter	Length	Thickness	Width
Compression	9 & 10	Pith	10.5 - 10.7	13.2 - 14.5	-	-
Creep (Lee et al., 2020)		Stem	11.6 - 12.1	18.5 - 18.7	-	-
Tensile Creep	3, 4, 5 & 6	Pith	-	73.4 - 107	1.37 - 2.77	2.81 - 6.36
		Rind	-	70.5 - 81.5	0.19 - 0.66	2.84 - 4.49

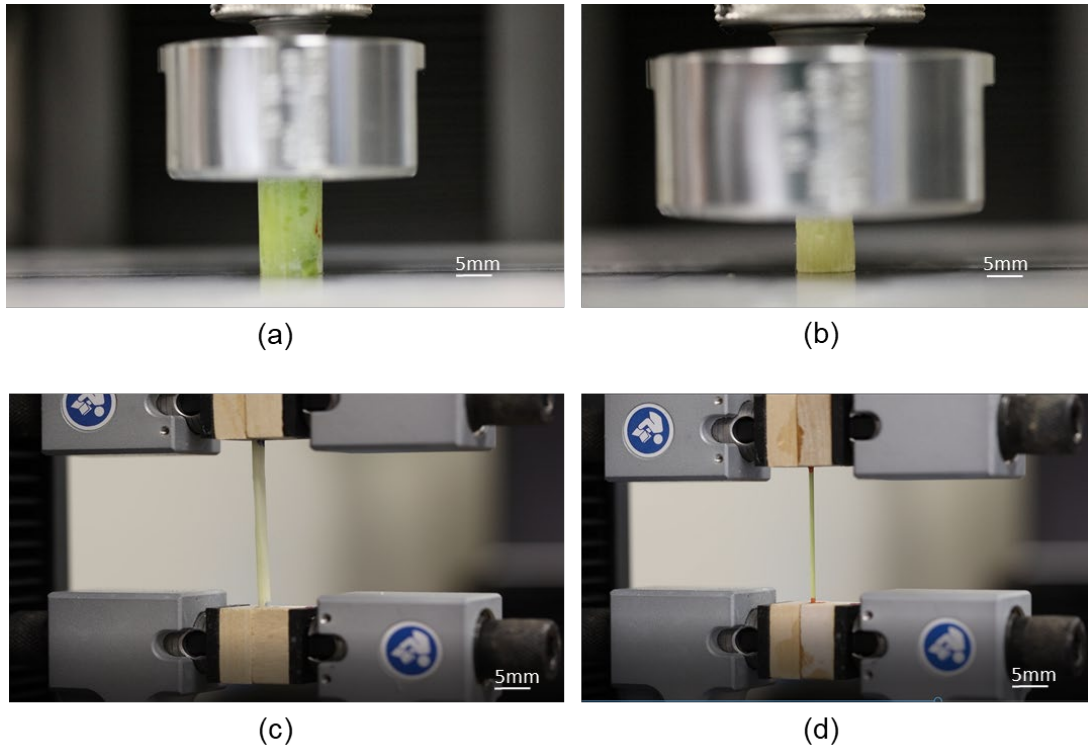
11

12 **2.3. Creep testing on stems and their constituents**

13 Uniaxial creep tests were conducted on the stems and their constituents (pith and rind) using an
 14 Instron 5943 with a 1 kN load cell for 1 hour at ~50% of the strength as measured from quasi-static ramp
 15 tests (at a loading rate of 1/min). All tests were performed at room temperature, ~23°C. A rigid test platen
 16 was implemented for the compression tests (Lee et al., 2020). In this setup, some lateral deformations can
 17 also occur at the top and bottom surfaces of the specimens, as they were not fixed (i.e., glued) to the platen
 18 (See **Figure 1a-b**). For the tensile tests, blocks were used to hold the specimens, with dimensions based on
 19 the sample thickness, to provide fixed boundary conditions and to avoid slippage issues at the grips (See
 20 **Figure 1c-d**). The samples were glued to the blocks using Loctite Super Glue (Al-Zube, Sun, Robertson,
 21 & Cook, 2018). The axial stress was calculated by dividing the measured force by the initial cross-sectional
 22 area of the specimens. The compressive specimens had a circular cross-section, while the tensile specimens
 23 had a rectangular cross-section. Compressive tests were performed on the entire stem and pith tissues, while
 24 tensile tests were performed on its constituents (pith and rind tissues). The strain was calculated by dividing
 25 the displacement of jaw fixtures by the initial distance between the grips (blocks). These quantities represent

1 nominal “engineering” stress and strain values of homogenized materials from ideal specimens (perfectly
2 straight and circular cross-section). As discussed above, plant tissues are composites of complex geometries
3 that experience non-uniform stress and strain fields within the specimens. Herein, we perform finite element
4 simulations to explore the influence of non-uniform stress and strain fields, geometric and material
5 variations, and testing boundary conditions on the overall quantification of the creep responses during
6 experiments.

7



8
9 Figure 1: Experimental set-up for (a) creep compression loading of a section of a stem, (b) creep
10 compression loading of a section of pith, (c) tensile creep loading of a section of pith, and (d) tensile creep
11 loading of a section of rind

12

13 **2.4. 3D Finite Element (FE) modeling of the stems**

14 To simulate creep responses of plant stems, a linear viscoelastic material model for isotropic
15 materials was considered and implemented using a UMAT subroutine in ABAQUS FE software. The
16 isotropic material was adopted due to limited available data since we only measured the uniaxial responses
17 in the experiments. If sufficient experimental data existed to capture the anisotropic and nonlinear
18 viscoelastic response of the plant stems and their constituents (rind, pith), a nonlinear viscoelastic model
19 for anisotropic materials (e.g., Sawant and Muliana (Sawant & Muliana, 2008), Song and Muliana (Song
20 & Muliana, 2019)) could be used. To examine the implications of isotropic and anisotropic mechanical

1 properties of stem tissues on the overall uniaxial and bending responses of plant stems, we performed
 2 simulations as discussed in **Appendix A**. It is seen that the effect of transversely isotropic properties on the
 3 uniaxial response relevant for the experimental test conducted is negligible. It is also seen that the
 4 transversely isotropic tissue properties have a negligible effect on the bending responses. The results are
 5 expected since under uniaxial loading and bending the deformations are mostly governed by the material
 6 responses along the longitudinal (axial) axis of the specimens. The linear viscoelastic model is expressed
 7 in terms of the deviatoric and volumetric strain components:

$$8 \quad \varepsilon_{ij}(t) = \frac{1}{2} \int_{0^-}^t J(t-s) \frac{dS_{ij}(s)}{ds} ds + \frac{1}{3} \delta_{ij} \int_{0^-}^t B(t-s) \frac{d\sigma_{kk}(s)}{ds} ds \quad (1)$$

9
 10 where $S_{ij}(t) = \sigma_{ij}(t) - \frac{1}{3} \delta_{ij} \sigma_{kk}(t)$ is the deviatoric stress component, $\sigma_{kk}(t)$ is the volumetric stress
 11 component, and δ_{ij} is the Kronecker delta. The shear and bulk creep compliances are given as
 12 $J(t) = 2(1 + \nu_o)D(t)$ and $B(t) = 3(1 - 2\nu_o)D(t)$, respectively, where ν_o is a Poisson's ratio, which is
 13 assumed constant, and $D(t)$ is the extensional creep compliance, given as:

$$14 \quad D(t) = \left(\frac{1}{E_0} + \sum_{i=1}^N \frac{1}{E_i} \left(1 - e^{\frac{-t}{\tau_i}} \right) \right) \quad (2)$$

15 where E_o is the instantaneous elastic modulus, N is the number of Prony terms, and E_i and τ_i are the
 16 time-dependent parameters to be used in the viscoelastic material model and the relaxation time,
 17 respectively, for each Prony term. The reason for using the Prony series for the memory kernel is due to its
 18 numerical advantage, in which the integral in Eq. (1) can be solved recursively, thereby reducing the
 19 computational cost. The disadvantage of using the memory kernel in Eq. (2) is due to its large number of
 20 material parameters required to capture the creep response. In addition, in the Prony series there is no
 21 uniqueness in the material parameters, where it is possible to have different combinations of characteristic
 22 times and weighting factors to fit the creep data. In this study, we started by picking the characteristic times
 23 in **Table 2** and then calibrated the parameters E_i by fitting the creep data. It is possible to pick slightly
 24 different characteristic times, as long as they are within the range of experimental data, and recalibrate the
 25 parameters E_i .

26 The stems were first simulated as perfect cylinders to extract the overall stress-strain responses,
 27 treating them as a homogenized body. For compression loading, two types of boundary conditions were
 28 chosen for the models while we applied pressure to the top surface: (1) free lateral sliding at the top and
 29 bottom surfaces and (2) fixed conditions at the top and bottom surfaces. For tensile testing, we considered

1 fixed conditions at both ends. For the compression and tension simulations, the model was meshed using
2 three-dimensional 8-node hexahedral linear brick (solid) elements. We also performed four-point bending
3 simulations in which the model was meshed using three-dimensional 20-node hexahedral quadratic brick
4 (solid) elements. Generally speaking, the stem specimens are not perfect cylinders, so simulations were
5 performed to investigate the influence of the actual stem geometries, as measured from real plants through
6 optical images, on the mechanical response. Simulations were also conducted to study how the properties
7 of the individual rind and pith constituents contribute to the overall mechanical response, i.e., as compared
8 to treating the stem as a homogeneous body.

9

10 **2.5. Data analysis**

11 Experimental data were extracted using the Instron software (Bluehill® Universal 4.01) and
12 processed in Microsoft Excel thereafter. Material properties were calibrated using the curve fitting tool in
13 Matlab® software and then imported in ABAQUS/CAE 2018. To calculate the ‘elastic moduli’ of the
14 specimens, the initial slopes under tensile and compression tests were calculated from 0 to 0.5% (linear
15 range) after implementing a toe correction method (Lee et al., 2020).

16

17 **3. Results**

18 In Sections 3.1 – 3.4, we explore the effect of geometric characteristics and boundary conditions
19 on the measured creep responses of sorghum stems. For this purpose, we considered creep responses from
20 compression testing of stems. In Sections 3.5 – 3.7, we elucidate the influence of different responses of pith
21 and rind on the overall creep responses of stems under compression, tension, and bending.

22

23 **3.1. Mesh size convergence study from creep compression of a perfect cylinder**

24 A mesh size study was carried out for a simple perfect cylinder (11.92 mm in diameter and 18.67
25 mm in height) to evaluate the stability of the finite element method. We considered fixed boundary
26 conditions at the top and bottom surfaces for the stem while applying a 1.9 MPa pressure load on the top
27 surface. Based on **Figure 2**, it can be seen that the von Mises stress converges (plateaus) above ~3000
28 elements. Specifically, using 3382 elements with an average element edge length of 1 mm is an optimal
29 mesh size.

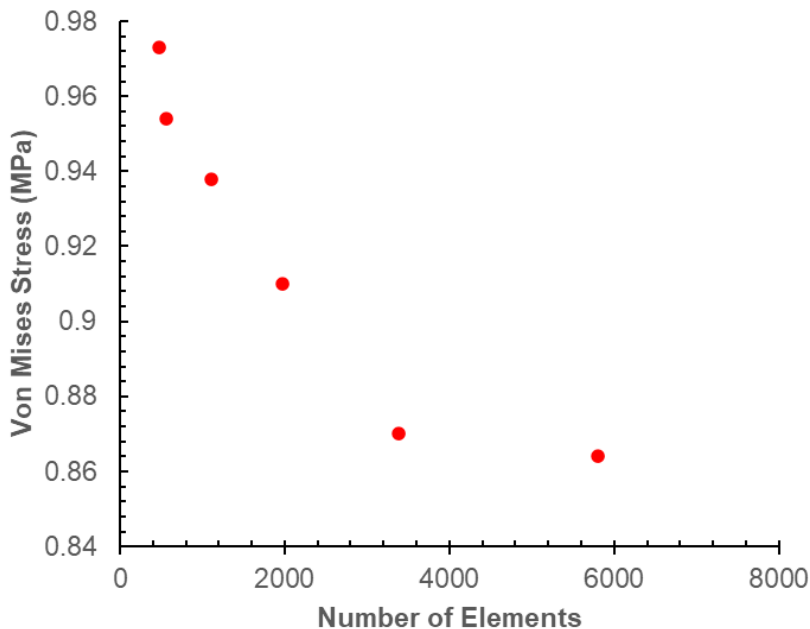


Figure 2: Results from a mesh-size convergence study from creep compression simulations of a perfect cylinder. The von Mises stress reported is at the center of the bottom surface of the stem. The stress converges (plateaus) above ~3000 elements.

3.2. Calibration of material parameters from creep compression testing of stems

The experimental data we used for calibrating material parameters from the compression creep responses represent the average response from three experimental creep tests of sorghum stems from our previous study (Lee et al., 2020). The elastic ‘instantaneous moduli’ of the specimens was calculated using the initial slopes under compression tests from 0 to 0.5% strain (linear range). Since we only extract the axial response in the experiments, we do not measure Poisson’s ratio. As such, we use a typical value of 0.25 for the Poisson’s ratio in the simulations (Stubbs et al., 2018). The time-dependent parameters for the stem were calibrated from experimental data (see Table 2). An applied stress of 1.9 MPa, which was used in the experiment, was prescribed to the model. Figure 3 shows the creep response from the experimental data and model from the material calibration. In conducting the calibration from the uniaxial compression data, the sorghum stem was treated as a homogenized body.

Table 2: Instantaneous moduli and time-dependent parameters of sorghum stem under creep compression loading (E_i to E_s are time-dependent parameters to be used in a viscoelastic material model)

i	τ_i (s)	E_i (MPa)
-----	--------------	-------------

1	0	-	54.0
2	1	5	582.8
3	2	50	317.8
4	3	500	569.3
4	4	5000	638.0
4	5	50000	141.9

5
6 The stem was first modeled as a perfect cylinder, 11.92 mm in diameter and 18.67 mm in height.
7 In our finite element analysis, we consider two boundary conditions that represent the limits of investigating
8 lateral deformation effects between the compression platen and the sample. One boundary condition
9 represents free sliding in the lateral direction, and the other boundary condition represents no sliding (full
10 constraint) in the lateral direction. For modeling the free sliding condition, the top and bottom surfaces of
11 the sample are constrained to uniformly move in the axial direction and are allowed to expand or contract
12 in the lateral direction. In this condition, the axial displacement field is uniform. The overall “engineering
13 strain” determined from the simulations with the two boundary conditions are nearly identical, and they are
14 comparable to experimental results (**Figure 3**). For the fully constrained boundary conditions where we
15 allow the sample to undergo bulging, strain localization occurs in the specimen, and hence the displacement
16 field varies through the sample (see **Figure 4**). These variations in strain fields through the specimen can
17 influence material parameter calibrations, as the overall “engineering strain” measure does not necessarily
18 represent the local strain field in the experiment. During our actual experiments, the boundary condition on
19 the top and bottom surfaces of the specimen is somewhere between the free sliding and fully constrained
20 limits.

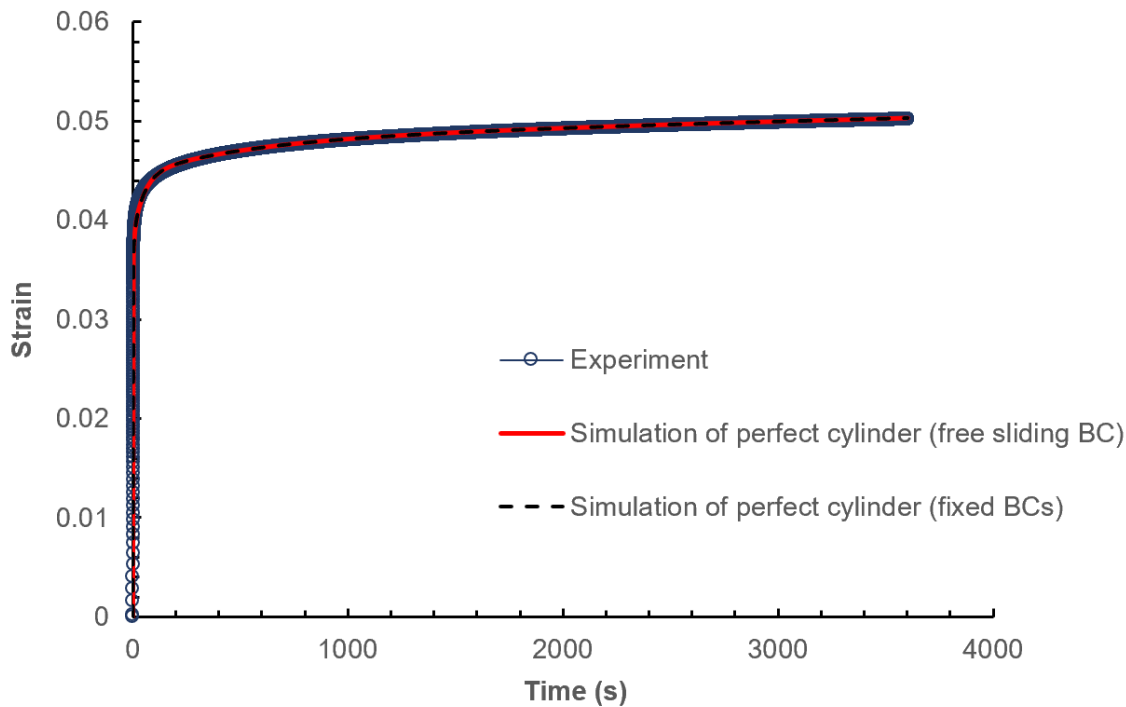


Figure 3: Modelling a perfect cylinder under creep compression loading of 1.9 MPa while considering free sliding and fixed boundary conditions.

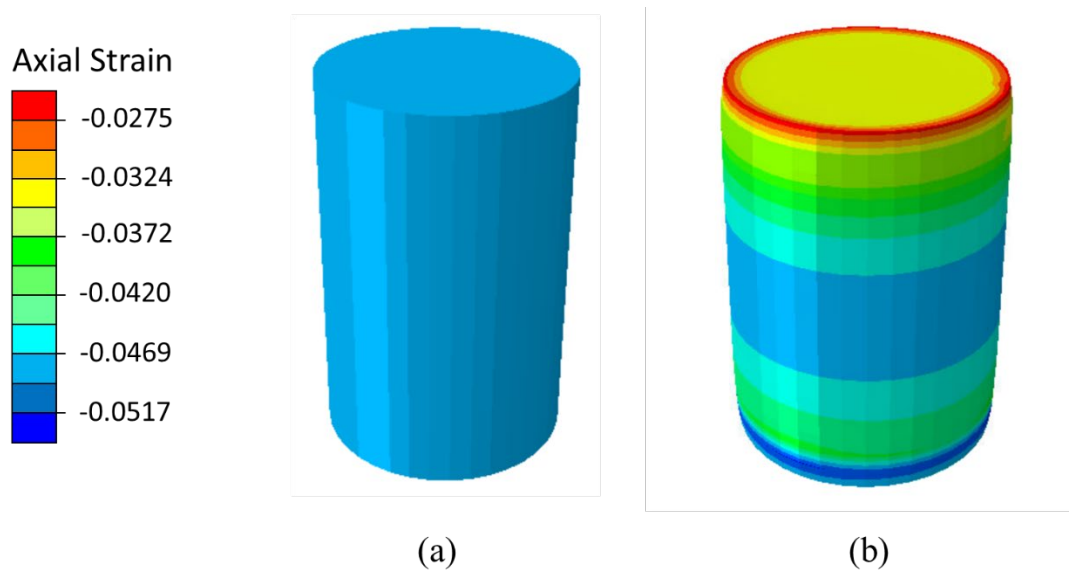
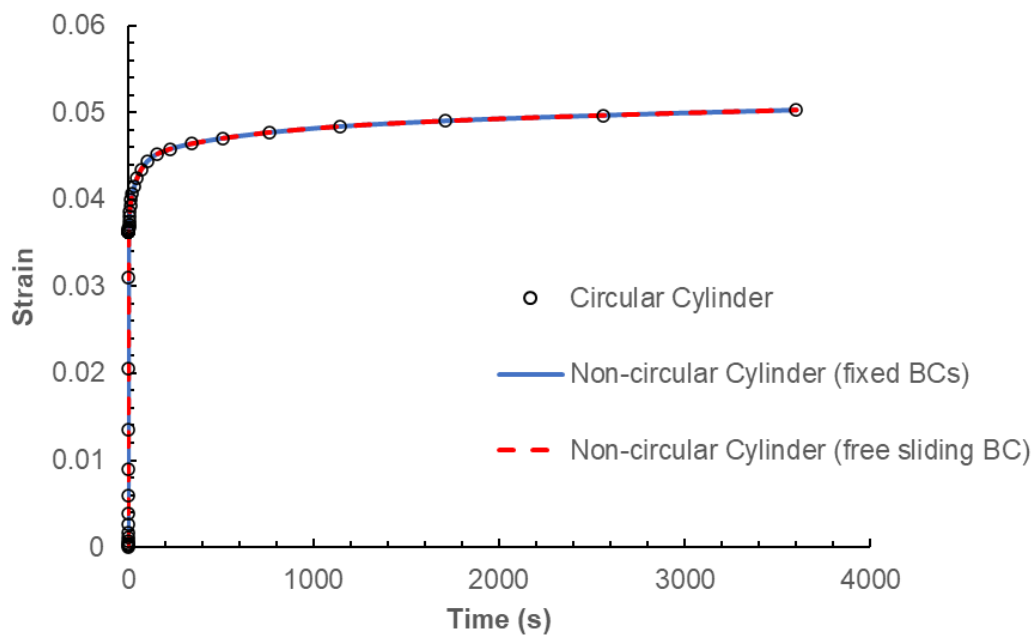


Figure 4: Axial strain contour plot for a simple cylinder model under creep compression at $t = 1000$ s for (a) free sliding boundary condition and (b) fixed boundary condition.

1 **3.3. Effects of non-circular cross-sections on compressive creep response of stems**

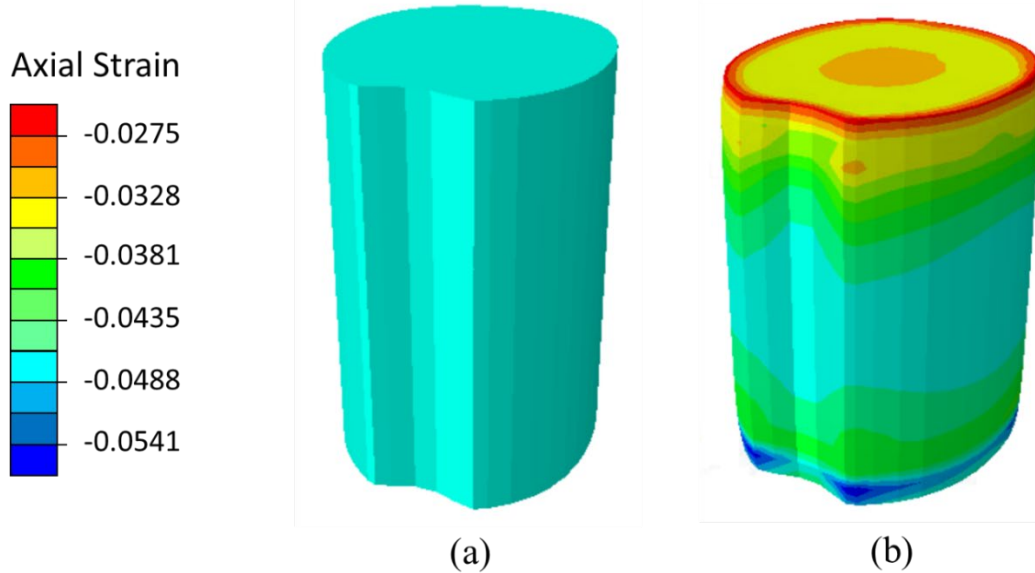
2 In this section, we investigate the effects of typical cross-sectional variations found among plants
3 on extracting the overall engineering stress-strain behavior from experiments. Generally speaking, the stem
4 dimensions and hence the distribution of the cross-section (shape) through the height of the sample might
5 affect the overall response. Since we obtained an optical image from the top of the plant, for simplification,
6 we focus on the top surface of the sample and assume that the cross-section maintains its shape through the
7 height of the sample. The total number of elements in the analysis was 3116. As before, we considered two
8 different boundary conditions: one of free sliding at the sample/platen interfaces, as to allow free lateral
9 deformation, and the other of constraining the lateral displacement of the sample at the sample/platen
10 interface. The result for free sliding at the platen interface is shown in **Figure 5**. Based on **Figure 5**, we can
11 see there is no change in the overall engineering strain output compared to the one from the simple cylinder
12 model, which indicates that the cross-sectional variation does not significantly affect the overall axial
13 deformation of the stem. For the fixed boundary conditions at the top/bottom surfaces, a spatial variation
14 occurs in the displacement field; strain localization changes the strain response by 17% at the bottom of the
15 sample and 49% at the top of the sample, as compared to the simple straight cylinder (percent difference)
16 (**Figure 6**).



17

18 **Figure 5:** Overall response during creep compression with free-sliding boundary conditions of a “real”
19 cylinder with a non-circular cross-section.

1



2

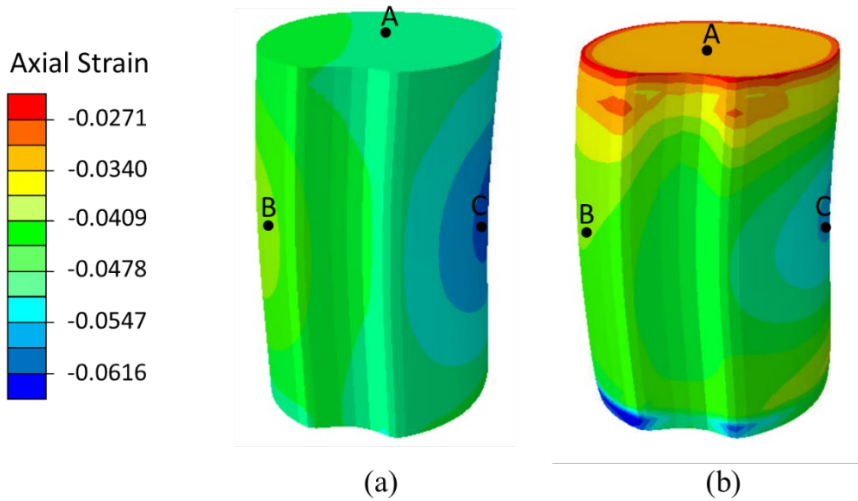
3 **Figure 6:** Axial strain contour plot of a “real” cylinder with non-circular cross-section under creep
 4 compression loading at time $t = 1000$ s for (a) free sliding boundary condition and (b) fixed boundary
 5 condition.

6

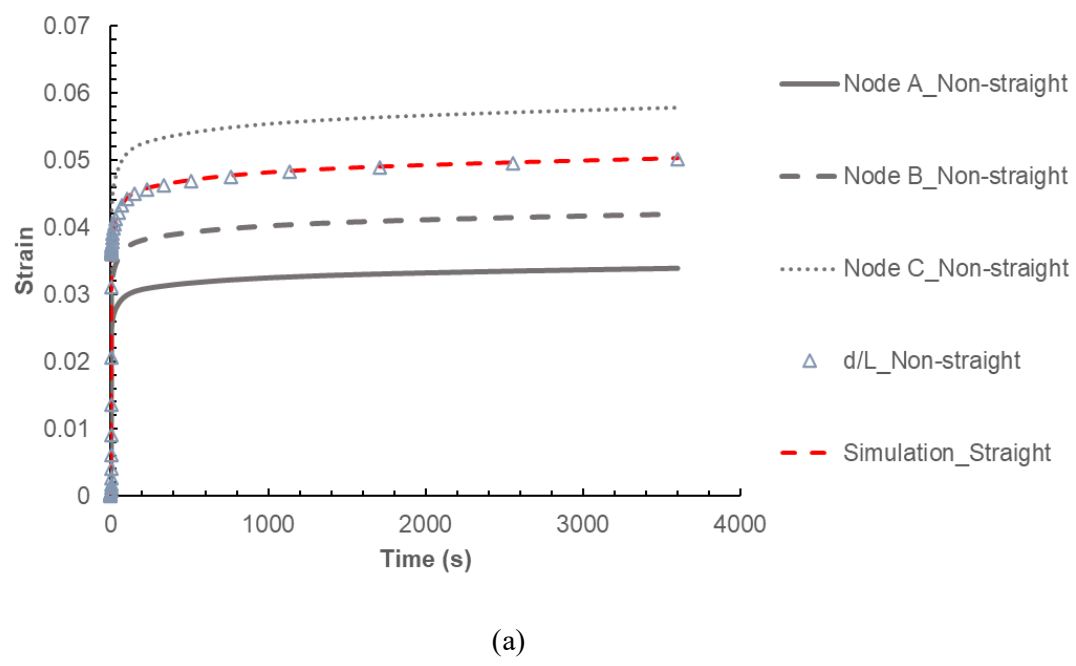
7 *3.4. Effect of non-straight specimens on the creep compression response*

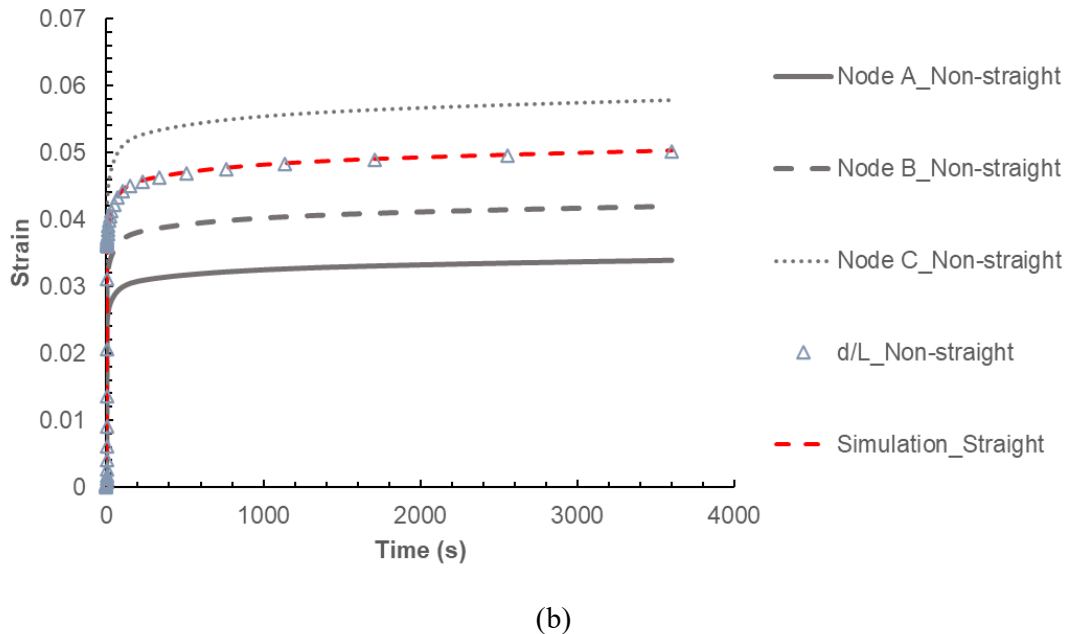
8 In this section, we use FE analysis to study the effect of samples that are not perfectly straight
 9 (along their long axis), which is common in plant stems, on extracting the overall engineering stress-strain
 10 behavior from mechanical testing. In reconstructing a real specimen, around 3 degrees of misalignment
 11 between the plant and the normal to the top/bottom surfaces was found to be typical in real plants (**Figure**
 12 **7**). The total number of elements in the analysis was 8175. Again, we considered the two boundary
 13 conditions as previously described. The strain field is seen in **Figure 7** for both the free sliding boundary
 14 condition (**Figure 7a**) and the fixed boundary condition (**Figure 7b**) for the realistic geometry. Strain
 15 localization occurs within the sample where the axial strain varies between 29% and 32% (relative percent
 16 difference) for the free sliding boundary condition and varies between 35% and 51% (relative percent
 17 difference) for the fixed boundary condition, as compared to the simple straight cylinder. The strain
 18 localization is due to the misalignment of the stem leading to bending and thus localized regions of tension
 19 and compression, even though the overall “engineering strain” through the dimension of the sample was
 20 found to be equivalent to the experimental data we have collected. **Figure 8a** shows the strain output at
 21 specific locations of the stem as indicated in **Figure 7** for the free sliding boundary condition, which
 22 indicates strain localization in certain regions. Likewise, **Figure 8b** shows strain localization at
 23 corresponding locations of the stem for the fully constrained boundary condition. The strain measure

1 determined from the experiments is based on the overall displacement (d/L , the “engineering strain”), while
 2 strains are field variables that can vary throughout the specimens. A large variation in strain response of
 3 Node A, B, and C can be also seen between the free sliding and fixed boundary conditions: 33%, 5.3%, and
 4 6.3% (relative percent difference), respectively.



5
 6 **Figure 7:** Axial strain contour plot of a “real” stem with an axial misalignment through the height (non-
 7 straight) under creep compression loading for a) free sliding and b) fixed boundary conditions at time $t =$
 8 1000 s.





(b)

Figure 8: Overall response during creep compression of a “real” stem with axial misalignment through the height (non-straight) with a) free-sliding boundary conditions, b) fixed boundary conditions,

3.5. Effects of different properties of the constituents (rind and pith) on compression creep tests

We next studied the influence of different properties of the individual constituents (rind and pith) on the overall creep compression of stems. Experimental tests were conducted on the pith tissue under creep compression. However, the rind is relatively thin, which made it impossible to do compression tests without inducing buckling. Comparing the pith and stem compressive responses (Lee et al., 2020), it is seen that the stems are much stiffer and stronger than the pith. We thus conclude that the stiffness and strength of the stems are largely due to the stiffer and stronger rind. Since the rind is quite stiff and does not exhibit significant creep compared to the pith (shown in the next section), we modeled the rind as linear elastic. For the pith, we calibrated time-dependent properties from creep compression tests (Table 3). The pith specimens were obtained from the same internodes as the stem specimens. Using FE simulations to match the instantaneous strain for the overall displacement (d/L) and the experiment, the elastic modulus of the rind was calibrated as approximately 325 MPa. Figure 9a shows the strain field within the stem with an elastic rind and a viscoelastic pith with a fixed boundary condition at the bottom surface. To mimic the compression experiment, a pressure is applied at the top surface of the rigid platen which is in contact with the sample (See Figure 9b). The contact between the platen and the sample was defined as a surface to surface contact interaction with a finite-sliding formulation and a hard penalty pressure-overclosure relationship considering tangential friction with a coefficient of friction of 0.2. The total number of elements

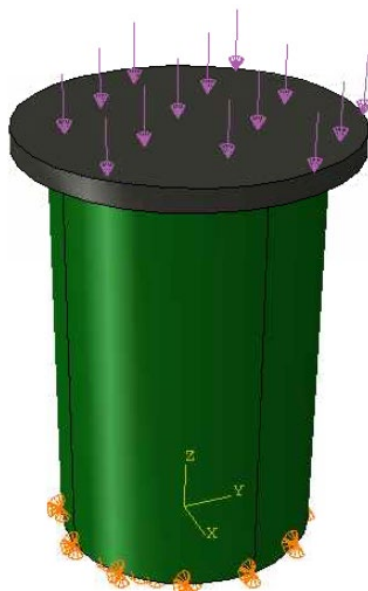
1 for the stem in the analysis was 6840. **Figure 10** shows the variation of strain locally within the stem. The
2 creep response of the pith constituent is also included for comparison. These results indicate that the overall
3 engineering strain obtained from the simulation (d/L) can capture the experimental creep responses.

4

5 **Table 3:** Instantaneous moduli and time-dependent parameters of sorghum pith under creep compression
6 (E_1 to E_5 are time-dependent parameters to be used in a viscoelastic material model)

i	τ_i (s)	E_i (MPa)
0	-	20.0
1	5	95.4
2	50	53.2
3	500	141.4
4	5000	499.5
5	50000	2.2

12



13

14 (a)

15

16

17

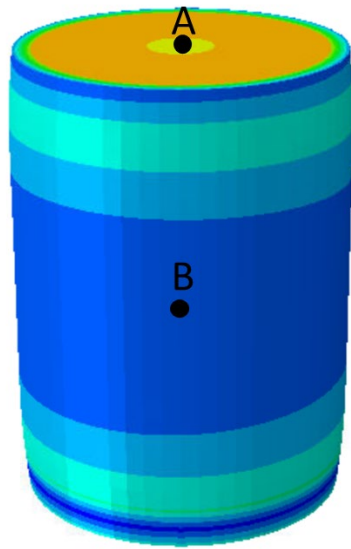
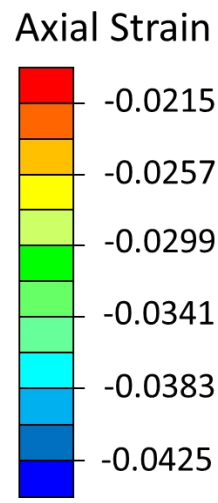


Figure 9: (a) Loading condition for the stem during compression creep (b) Axial strain contour plot of a stem undergoing compression creep loading, assuming the pith as viscoelastic material and the rind as a linear elastic material with a modulus of 325 MPa and fixed boundary conditions at time $t = 1000$ s.

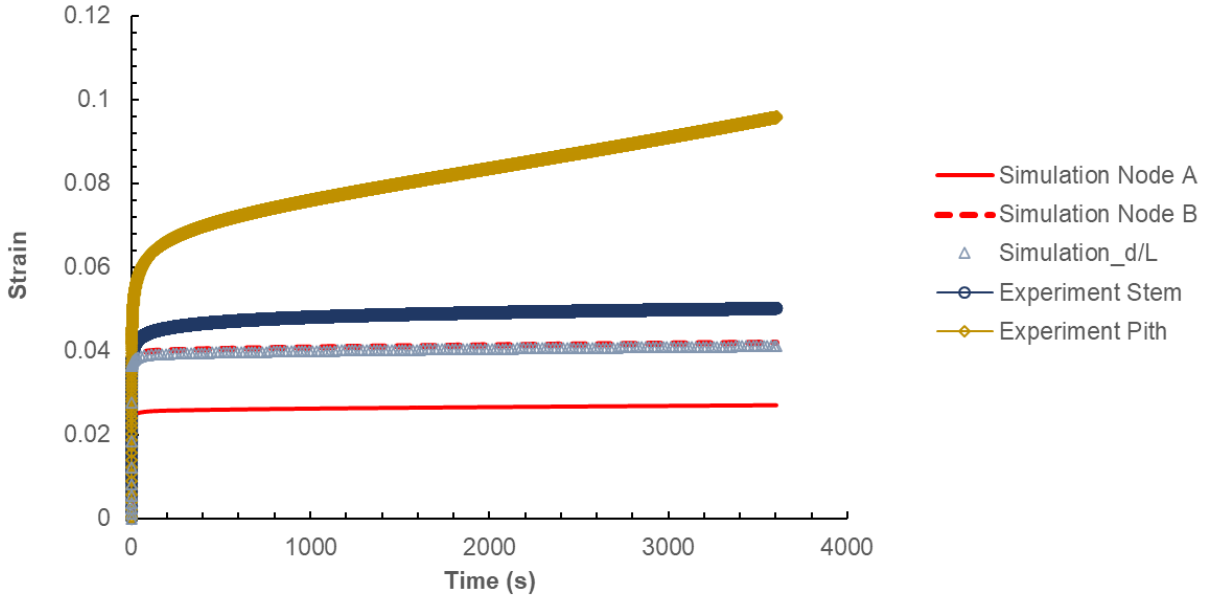
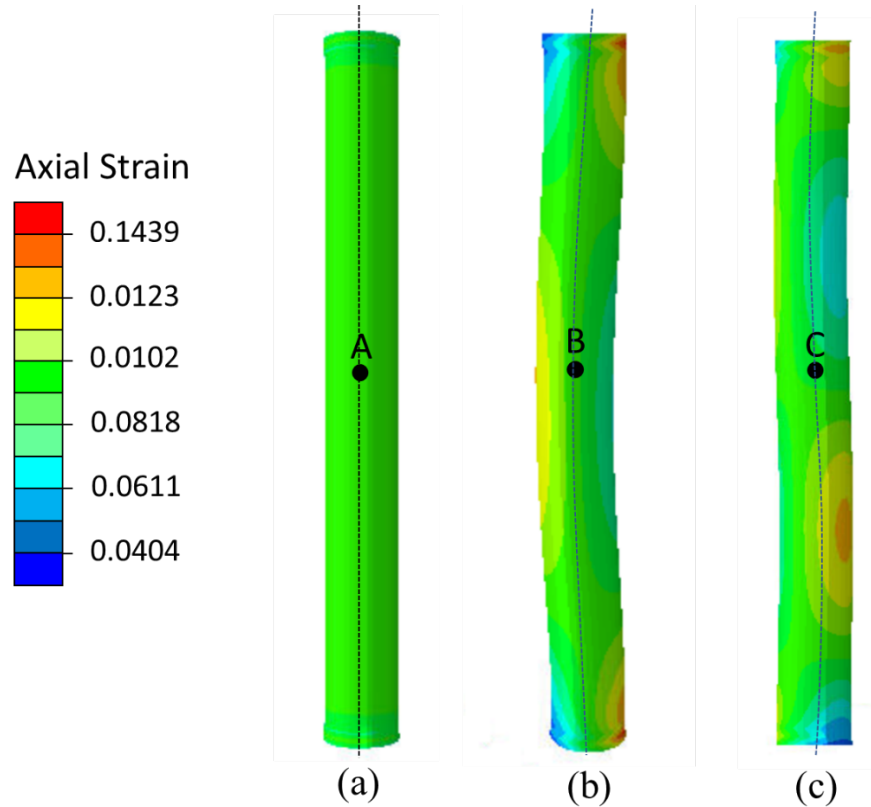


Figure 10: Overall response of a stem under creep compression loading of 1.9 MPa, assuming the pith as viscoelastic material and rind as a linear elastic material with a modulus of 325 MPa with fixed boundary conditions

1 **3.6. Simulating tension responses**

2 We now analyze the influence of tension responses of the individual constituents (rind and pith) on
3 the overall tension behavior of the stem. The pith and rind properties were calibrated and shown in **Tables**
4 **4 and 5**, respectively. The internode length and diameter were measured as 102 mm and 11.9 mm,
5 respectively, and the thickness of the rind was measured as 0.62 mm. As mentioned in previous studies
6 distinguishing between the rind and pith is somewhat challenging, as the boundaries are not distinct (Stubbs,
7 Sun, & Cook, 2019). Herein we identified the boundaries using optical images of the stem cross-section
8 simply by considering rind as dark green tissue and pith as a light green region through the RGB color
9 analyzer (using a threshold for light green and dark green), as to estimate the thickness of the rind. The
10 elastic moduli for the pith and rind were calibrated as 20 MPa and 580 MPa, respectively. The creep stress
11 levels (defined as the stress at 50% of the strength) for pith and rind were 0.8 MPa and 18.5 MPa,
12 respectively. The stem was assumed to be fixed at both ends while we apply external tensile loading at the
13 top surface. In the simulations, we use external stress of 1.1 MPa to ensure that the produced stress in the
14 pith constituent is smaller than the strength of the pith (1.6 MPa). Three different geometries were modeled.
15 **Figures 11a-c** show the strain contours in a straight cylinder with a non-circular cross-section (A), a non-
16 circular cylinder with a single curvature through the height (B), and a non-circular cylinder with two
17 curvatures through the height (C). The total number of elements for the non-circular straight cylinder, non-
18 circular cylinder with a single curvature, and non-circular cylinder with two curvatures was 21,012, 13,940,
19 and 11,135, respectively. For the straight non-circular cross-section, the strain contour is uniform; however,
20 for the other two cases, the strain varies through the height due to the non-uniform geometry. **Figure 12**
21 shows the overall response of the stems due to external loading. As seen in **Figure 12**, the “engineering
22 strains (d/L)” for all cases (corresponding to models (A)-(C) in **Figure 11**) are similar; however, there is a
23 larger variation in the local axial strain responses among the specimens, which as an example is shown by
24 the strains at the center location on the free lateral surface of the stem. These slight variations in the tensile
25 responses from the geometries of the stems can influence the material parameter characterizations.

26



1

2 **Figure 11:** Axial strain contour plot of a stem undergoing tensile creep loading, assuming the pith and rind
 3 as viscoelastic materials with fixed boundary conditions at time $t = 1000$ s for a) perfect non-circular
 4 cylinder, b) a non-circular cylinder with a curve through the height, and c) a non-circular cylinder with two
 5 curves through the height.

6

7 **Table 4:** Instantaneous moduli and time-dependent parameters of sorghum pith under creep tensile loading
 8 (E_1 to E_5 are time-dependent parameters to be used in a viscoelastic material model)

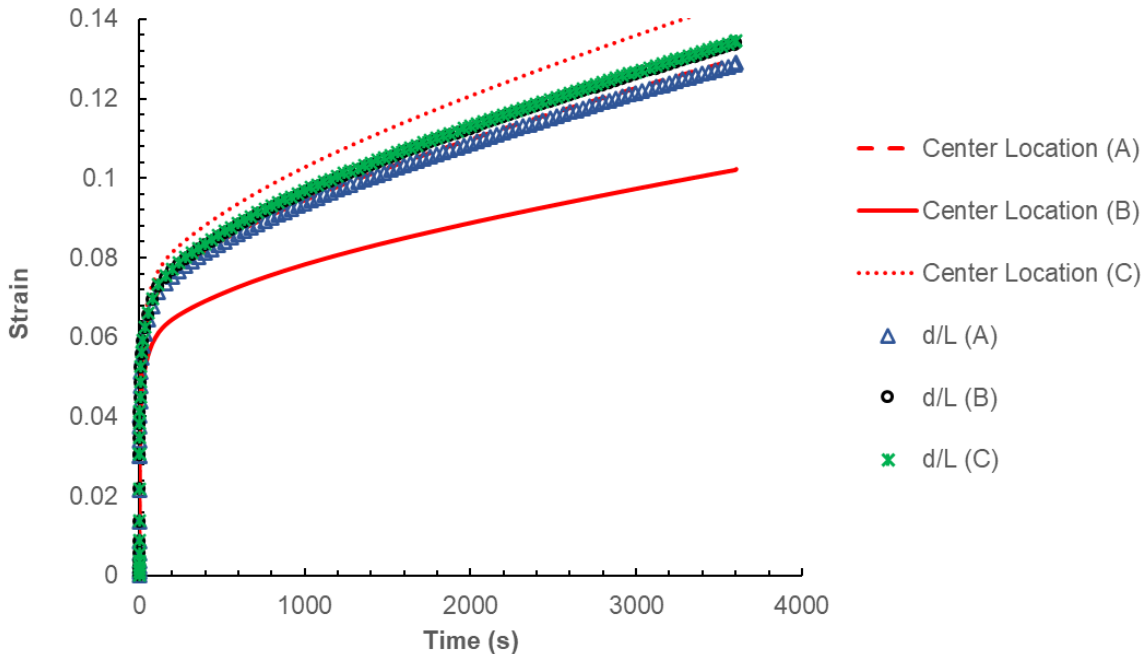
i	τ_i (s)	E_i (MPa)
0	-	20.0
1	5	16.02
2	50	30.3
3	500	66.28
4	5000	29.73
5	50000	4.602

15

16

1 **Table 5:** Instantaneous moduli and time-dependent parameters of sorghum rind under creep tensile loading
 2 (E_1 to E_5 are time-dependent parameters to be used in a viscoelastic material model)

i	τ_i (s)	E_i (MPa)
0	-	580
1	5	606
2	50	751
3	500	1118
4	5000	625
5	50000	1062



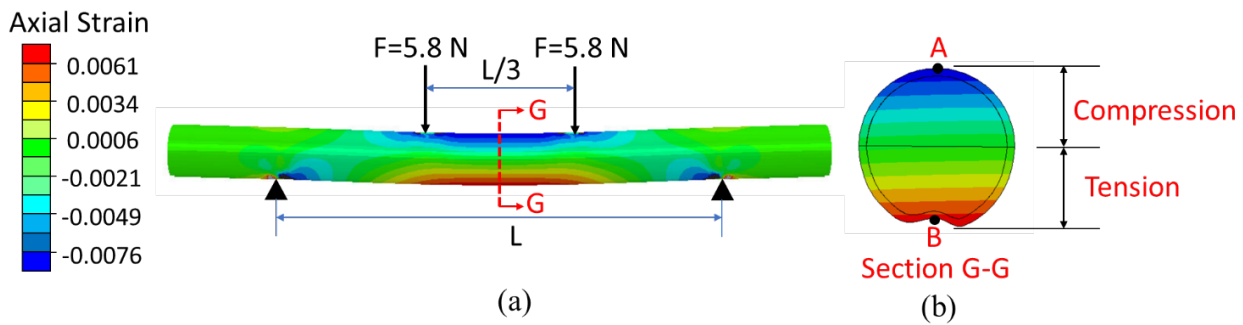
10 **Figure 12:** Overall response of the stem under creep tensile loading of 1.1 MPa for cases a-c (from Fig. 9).

11 12 **3.7. Simulating bending responses**

13 As previously mentioned, a prominent failure mode in plant lodging is associated with bending of
 14 the stems (see **Figure 13**). We thus analyze the creep bending response of a sorghum stem during a 4-point
 15 bending test by incorporating tension and compression properties we calibrated from the previous sections.
 16 In other words, for the region under compression (top), we assigned viscoelastic and elastic properties to
 17 the pith and rind, respectively; however, for the region under tension (bottom), we used viscoelastic
 18 properties for both pith and rind (See **Figure 13b, d, f**). As in the previous section we consider three

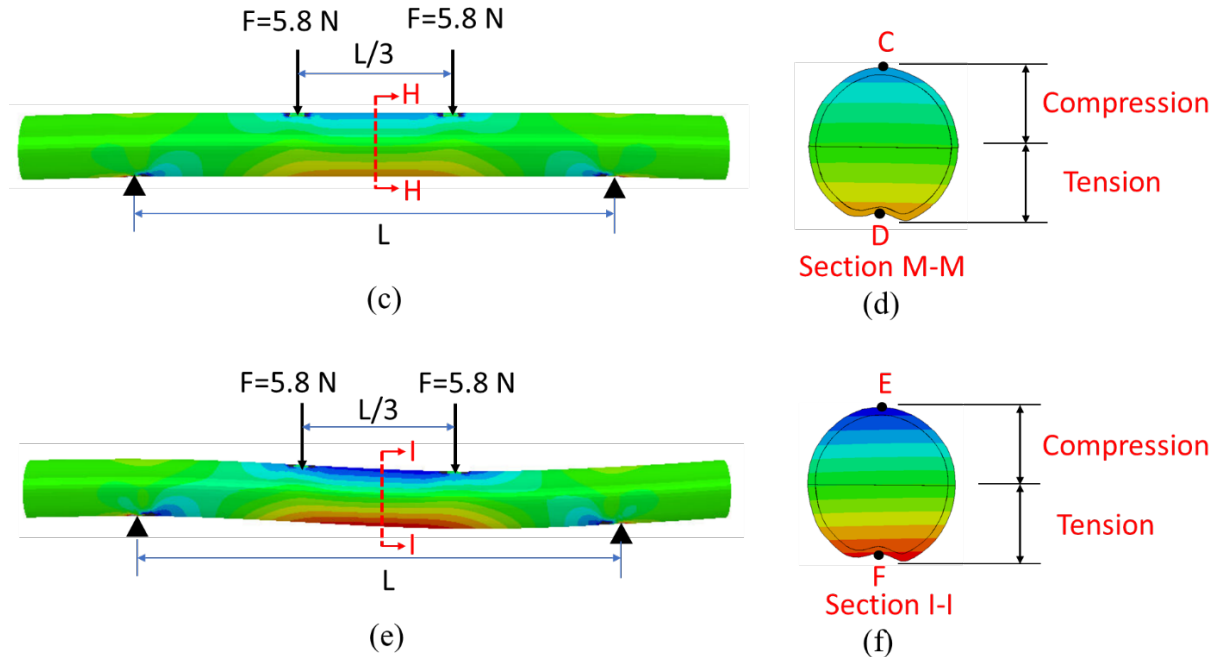
1 different geometries: a non-circular straight cylinder (**Figure 13a**), a non-circular cylinder with a slight
 2 curve through the height (**Figure 13c**), and a non-circular cylinder with two slight curves through the height
 3 (**Figure 13e**). These figures show the longitudinal strain contour through the stem. The applied force is
 4 calibrated through FE analysis in such a way that the corresponding stress in the rind in the tension region
 5 correlates with the same stress level as the rind in the uniaxial tensile testing we have discussed before.
 6 **Figure 14** also shows the longitudinal strain response of the stem due to creep bending at two different
 7 regions (Nodes A-F) for three different geometries (non-circular straight cylinder, non-circular cylinder
 8 with a slight curve, and non-circular cylinder with two slight curves). We can see that at nodes C and E
 9 (compression locations), the longitudinal strain variation is 38% for the stem with a slight curve and 100%
 10 for the stem with two slight curves, as compared to straight stem (node A) (percent difference). This
 11 difference for nodes D and F (tension regions) is 39% for the stem with a slight curve and 9.4% a stem with
 12 two slight curves, as compared to the straight stem (node B).

13



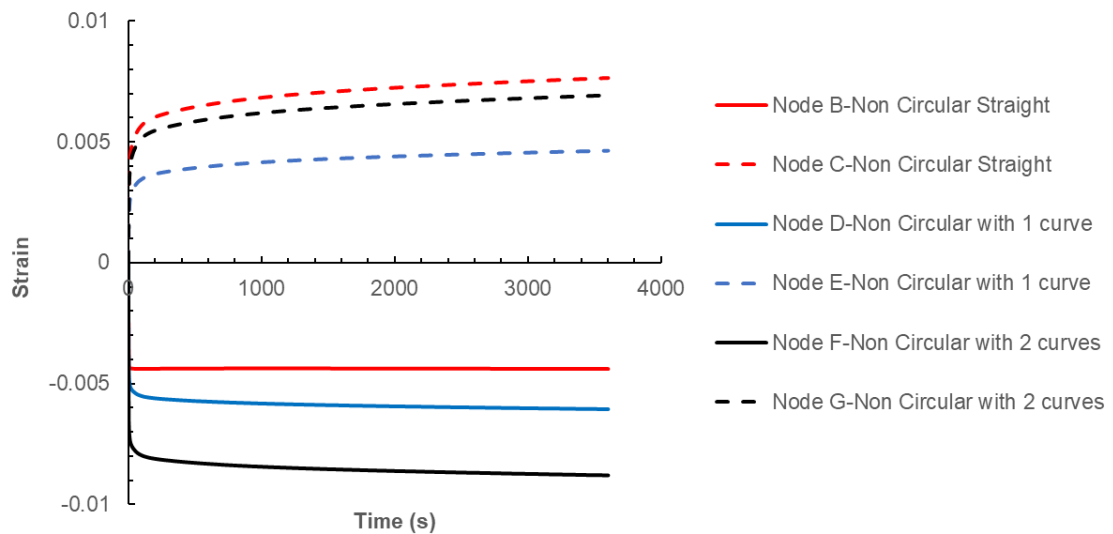
14

15



1

2 **Figure 13:** Longitudinal (axial) strain contour of the stem under creep bending loading at $t = 1000$ s: a)
3 perfect non-circular straight cylinder, b) cross-section for non-circular straight cylinder, c) non-circular
4 cylinder with a slight curve through the height, d) cross-section for non-circular cylinder with a slight curve,
5 e) a non-circular cylinder with two curves through the height, and f) cross-section for non-circular cylinder
6 with two curves through the height.



7

8 **Figure 14:** Overall response of the stem under creep bending loading at nodes A through F.

9

1 **4. Discussion**

2 In this study, we investigated the effects of boundary conditions and geometric variations on the
3 overall creep behavior of the sorghum stems to examine the influence of these variables on the experimental
4 data, which were used to calibrate material parameters. In terms of geometric variations typically found in
5 sorghum stems, we can conclude that cross-sectional variations and curvatures along the longitudinal axis
6 (whether they are straight or not) do not change the overall engineering compressive and tensile strain.
7 However, these geometric variations result in large local differences in stresses and strains. For instance, in
8 a sorghum stem misaligned through the height (non-straight), bending will occur when applying uniaxial
9 compression loading. For compression loading, deviations in strains from straight cylinders are higher while
10 using a free sliding boundary condition which is up to 23% and 21% (percent difference) in compression
11 and tension regions, as compared to the straight sample. In terms of tensile responses, a slight curve (by 3
12 degrees with respect to the longitudinal axis) changes the strain response up to 21% in the middle surface,
13 and two slight curves through the height of the sample can change the response up to 11% (percent
14 differences). Similarly, in bending, a slight curve through the height changes the strain response in the
15 middle cross-section up to 39% in tension regions and 38% in compression regions. Having two slight
16 curves through the height changes the strain response up to 9.4% in tension regions and 100% in
17 compression regions (percent differences). This localized strain is important for predicting failure of the
18 stem. From these simulations, we can conclude that using the ‘engineering stress-strain’ measures under
19 tension and compression tests can only give us ‘average’ mechanical properties of the stems. The localized
20 stress/strain that occurs in the specimens can potentially lead to localized failures at local stresses/strains
21 that are much larger than those detected (i.e., measured) from the average mechanical responses of the
22 stems. Under bending, the localized strain (and stress) responses are sensitive to the geometrical parameters
23 of the stems, which can significantly affect the calibrated material parameters. Thus, we conclude that to
24 properly extract the material parameters from the standard mechanical testing procedures, i.e., compression,
25 tension, and bending, it is necessary to model the geometry of the samples properly. More precise
26 representations of the geometry can be obtained from optical image of the tested specimens, as implemented
27 in this study.

28 In terms of boundary conditions, we observed that for a non-circular straight cross-section, the free
29 sliding boundary condition does not affect the strain response but the fixed boundary condition does affect
30 the local strain response, as compared to a circular cross-section. For non-straight samples, both boundary
31 conditions influence the local strain response. In all cases, the “engineering strain” that we measure in the
32 experiment matches the overall longitudinal strain in the simulations (d/L). However, strain is a field
33 variable, and hence there are local variations in the strain that vary depending on the boundary conditions.

1 For a non-straight stem, the free sliding boundary condition could change the compressive responses up to
2 0.2% at the top surface while this difference is up to 33% for the fixed boundary condition compared to
3 straight stem. While in the actual experiments, the boundary condition on the top and bottom surfaces of
4 the specimen is somewhere between the free sliding and fully constrained limits, it is very challenging (if
5 not impossible) to determine the exact “correct” boundary condition in the experiment. This issue might
6 have consequences in determining the overall mechanical properties of the stems.

7 We also studied the overall tensile, compressive, and bending response of the stem, considering the
8 pith and rind properties individually. Based on the compressive responses, we found that although the rind
9 supports the majority of the load and does not creep significantly itself, the pith does, and hence, we get
10 overall creep in the stem. Even though the applied load is constant, the resulting stress in the pith and rind
11 evolves in time due to the creep of the pith and to maintain the equilibrium condition. Therefore, assuming
12 the rind as an elastic component seems to be a reasonable approximation (recall that compression
13 experiments on the rind are cumbersome or impossible). The bending results indicate that by incorporating
14 tensile and compressive creep properties for the corresponding rind and pith constituents, an overall creep
15 response for the stem can be predicted, in which the predicted longitudinal strain as a function of position
16 could be used to predict stem lodging.

17

18 **5. Limitations**

19 As we are testing fresh samples, there is a possibility of water loss during the specimen preparation
20 prior to testing. To minimize water loss, we ensured that all samples were tested within 6 hours from cutting
21 them from the plants. However, it is possible that some water loss did occur in this 6-hour window. Future
22 studies should include weighing the specimens immediately after cutting them from the plants and
23 immediately prior to each mechanical test.

24 The creep tests were performed for one hour, which is a relatively short term. This short-term test
25 was performed since we tested fresh samples, and longer-term creep tests (e.g., days) may cause water loss
26 from evaporation. Future studies may consider long-term creep tests of fresh stems, which is also important
27 in accounting for other physical process such as water migration during testing.

28

29 **6. Conclusions**

30 In this study, we conducted experimental creep tests on sorghum stems, piths, and rinds. We also
31 investigated the biomechanical response of sorghum stem through finite element analysis to analyze the

1 effects of geometric irregularities in plants (deviations in cross-sectional and longitudinal shape from
2 perfect circular cylinders), as well as any potential artifacts associated with boundary conditions during
3 mechanical testing. Through finite element simulations, we show that the typical differences found in cross-
4 sectional shapes of stems and curvatures through the stem height (e.g., a 3-degree deviation from straight
5 cylinders) have a negligible influence on the average tension and compression responses of the stem during
6 mechanical testing. However, finite element analysis indicated that these variations do alter the local strain
7 at specific key locations relative to a perfect circular cylinder (up to 33% and 23% for fixed and free sliding
8 boundary conditions, respectively). Failure may occur prematurely during testing due to these effects, as
9 stresses will develop that readily exceed the strength of the plant locally prior to what is measured globally.
10 We also determined that although the rind supports the majority of the load and does not creep significantly
11 itself, the pith does, and hence we get overall creep in the stem. Overall, even though geometrical
12 irregularities in sorghum stems present challenges, mechanical testing is still useful in extracting overall
13 (average) mechanical responses of the stems under compression, tension, and bending. Finite element
14 models with realistic stem geometries can improve the fidelity in extracting mechanical properties in these
15 tests. In the future, full-field measurement testing and/or localized testing, e.g., indentation, may prove
16 useful in providing more accurate measurements of the biomechanical properties of stems. The full-field
17 measurement and/or localized testing will require the corresponding testing simulation (digital twin or
18 virtual testing approach) to properly extract material properties.

19

20 Acknowledgments

21 This research is sponsored by the National Science Foundation under grant CMMI-1761015. We provide a
22 special thanks to Qing Li who grew the sorghum for biomechanical testing. We also thank Dr. Scott A.
23 Finlayson for his valuable advice during this project. The finite element analyses were conducted at the
24 Texas A&M's High-Performance Research Computing Center. This support is gratefully acknowledged.

25

26 References

27

28 Al-Zube, L. A., Robertson, D. J., Edwards, J. N., Sun, W., & Cook, D. D. (2017). Measuring the
29 compressive modulus of elasticity of pith-filled plant stems. *Plant Methods*, 13(1), 99.

30 Al-Zube, L. A., Sun, W., Robertson, D., & Cook, D. D. (2018). The elastic modulus for maize stems.
31 *Plant Methods*, 14(1), 11.

32 Alméras, T., Gril, J., & Costes, E. (2002). Bending of apricot tree branches under the weight of axillary
33 growth: test of a mechanical model with experimental data. *Trees*, 16(1), 5-15.

34 Berry, P., Sterling, M., Spink, J., Baker, C., Sylvester-Bradley, R., Mooney, S., . . . Ennos, A. (2004).
35 Understanding and reducing lodging in cereals. *Advances in agronomy*, 84(04), 215-269.

1 Boubakar, M., Vang, L., Trivaudey, F., & Perreux, D. (2003). A meso-macro finite element modelling of
2 laminate structures: Part II: time-dependent behaviour. *Composite structures*, 60(3), 275-305.

3 Bozorg, B., Krupinski, P., & Jönsson, H. (2014). Stress and strain provide positional and directional cues
4 in development. *PLoS computational biology*, 10(1), e1003410.

5 Cisse, O., Placet, V., Guicheret-Retel, V., Trivaudey, F., & Boubakar, M. L. (2015). Creep behaviour of
6 single hemp fibres. Part I: viscoelastic properties and their scattering under constant climate.
7 *Journal of materials science*, 50(4), 1996-2006.

8 De Tommasi, D., Puglisi, G., & Saccomandi, G. (2006). A micromechanics-based model for the Mullins
9 effect. *Journal of Rheology*, 50(4), 495-512.

10 Edelmann, H. G., & Köhler, K. (1995). Auxin increases elastic wall-properties in rye coleoptiles:
11 implications for the mechanism of wall loosening. *Physiologia Plantarum*, 93(1), 85-92.

12 Gomez, F. E., Carvalho, G., Shi, F., Muliana, A. H., & Rooney, W. L. (2018). High throughput
13 phenotyping of morpho-anatomical stem properties using X-ray computed tomography in
14 sorghum. *Plant Methods*, 14(1), 59.

15 Gomez, F. E., Muliana, A. H., Niklas, K. J., & Rooney, W. L. (2017). Identifying morphological and
16 mechanical traits associated with stem lodging in bioenergy sorghum (*Sorghum bicolor*).
17 *BioEnergy Research*, 10(3), 635-647.

18 Gomez, F. E., Muliana, A. H., & Rooney, W. L. (2018). Predicting stem strength in diverse bioenergy
19 sorghum genotypes. *Crop Science*, 58(2), 739-751.

20 Hirano, K., Ordonio, R. L., & Matsuoka, M. (2017). Engineering the lodging resistance mechanism of
21 post-Green Revolution rice to meet future demands. *Proceedings of the Japan Academy, Series B*,
22 93(4), 220-233.

23 Kaplan, J., Torode, T., Daher, F. B., & Braybrook, S. (2019). On pectin methyl-esterification:
24 Implications for in vitro and In vivo viscoelasticity. *BioRxiv*, 565614.

25 Kin, K., & Shim, K. (2010). Comparison between tensile and compressive Young's modulus of structural
26 size lumber. Paper presented at the World conference on timber engineering. Riva del Garda,
27 Italy.

28 Kutschera, U., & Briggs, W. R. (1987). Differential effect of auxin on in vivo extensibility of cortical
29 cylinder and epidermis in pea internodes. *Plant Physiology*, 84(4), 1361-1366.

30 Kutschera, U., & Briggs, W. R. (1988). Growth, in vivo extensibility, and tissue tension in developing pea
31 internodes. *Plant Physiology*, 86(1), 306-311.

32 Kutschera, U., & Schopfer, P. (1986). In-vivo measurement of cell-wall extensibility in maize coleoptiles:
33 Effects of auxin and abscisic acid. *Planta*, 169(3), 437-442.

34 Lee, S., Zargar, O., Reiser, C., Li, Q., Muliana, A., Finlayson, S. A., . . . Pharr, M. (2020). Time-
35 dependent mechanical behavior of sweet sorghum stems. *Journal of the Mechanical Behavior of
36 Biomedical Materials*, 103731.

37 Lemloh, M.-L., Pohl, A., Zeiger, M., Bauer, P., Weiss, I. M., & Schneider, A. S. (2014). Structure-
38 property relationships in mechanically stimulated Sorghum bicolor stalks. *Bioinspired Materials*.

39 Niu, L., Feng, S., Ding, W., & Li, G. (2016). Influence of speed and rainfall on large-scale wheat lodging
40 from 2007 to 2014 in China. *Plos One*, 11(7), e0157677.

41 Robertson, D. J., Julias, M., Lee, S. Y., & Cook, D. D. (2017). Maize stalk lodging: morphological
42 determinants of stalk strength. *Crop Science*, 57(2), 926-934.

43 Robertson, D. J., Smith, S. L., & Cook, D. D. (2015). On measuring the bending strength of septate grass
44 stems. *American journal of botany*, 102(1), 5-11.

45 Sawant, S., & Muliana, A. (2008). A thermo-mechanical viscoelastic analysis of orthotropic materials.
46 *Composite structures*, 83(1), 61-72.

47 Shah, D. U., Reynolds, T. P., & Ramage, M. H. (2017). The strength of plants: theory and experimental
48 methods to measure the mechanical properties of stems. *Journal of Experimental Botany*, 68(16),
49 4497-4516.

50 Song, R., & Muliana, A. (2019). Modeling mechanical behaviors of plant stems undergoing
51 microstructural changes. *Mechanics of Materials*, 139, 103175.

1 Stubbs, C. J., Baban, N. S., Robertson, D. J., Alzube, L., & Cook, D. D. (2018). Bending stress in plant
2 stems: models and assumptions. In *Plant Biomechanics* (pp. 49-77): Springer.

3 Stubbs, C. J., Sun, W., & Cook, D. D. (2019). Measuring the transverse Young's modulus of maize rind
4 and pith tissues. *Journal of biomechanics*, 84, 113-120.

5 Suslov, D., & Verbelen, J. (2006). Cellulose orientation determines mechanical anisotropy in onion
6 epidermis cell walls. *Journal of Experimental Botany*, 57(10), 2183-2192.

7 Wirawan, R., Sapuan, S., Robiah, Y., & Khalina, A. (2011). Elastic and viscoelastic properties of
8 sugarcane bagasse-filled poly (vinyl chloride) composites. *Journal of thermal analysis and*
9 *calorimetry*, 103(3), 1047-1053.

10 Wright, C. T., Pryfogle, P. A., Stevens, N. A., Steffler, E. D., Hess, J. R., & Ulrich, T. H. (2005).
11 Biomechanics of wheat/barley straw and corn stover. *Applied biochemistry and biotechnology*,
12 121(1-3), 5-19.

13 Yuan, Z., Muliana, A., & Rajagopal, K. (2020). Modeling deformation induced anisotropy of light-
14 activated shape memory polymers. *International Journal of Non-Linear Mechanics*, 120, 103376.

15 Zeng, X., Mooney, S. J., & Sturrock, C. J. (2015). Assessing the effect of fibre extraction processes on the
16 strength of flax fibre reinforcement. *Composites Part A: Applied Science and Manufacturing*, 70,
17 1-7.

18 Zuber, M., Colbert, T., & Darrah, L. (1980). Effect of Recurrent Selection for Crushing Strength on
19 Several Stalk Components in Maize 1. *Crop Science*, 20(6), 711-717.

20

21

1 Appendix A 2

3 This Appendix discusses simulation results for investigating the influence of material anisotropy
4 on uniaxial loading and bending of plant stems, following typical experimental tests. The stems are modeled
5 as a composite material having rind (outer layer) and pith (inner core) tissues. For each uniaxial
6 compression and bending case, three material behaviors were considered. The first two cases (Case (a) and
7 Case (b)) consider both pith and rind as transversely isotropic materials. As we pointed out that we were
8 limited in obtaining multi-axial material properties for the sorghum stems, we referred to (Bozorg,
9 Krupinski, & Jönsson, 2014) and (Kaplan, Torode, Daher, & Braybrook, 2019) in determining the
10 transversely isotropic properties of the tissues. Kaplan et al. (Kaplan et al., 2019) discussed that for the
11 studied *Arabidopsis* cell walls, the transverse modulus is stiffer than the axial modulus (315 ± 46 kPa for
12 axial walls compared to 488 ± 104 kPa for transverse walls), while Bozorg et al. (Bozorg et al., 2014) in
13 their simulation of plant cell wall used the transverse modulus to be half of the axial modulus (12 GPa for
14 the axial modulus and 6 GPa for the transverse modulus). In our simulations we considered the transverse
15 modulus to be twice of the axial modulus for Case (a), while for Case (b) we considered the transverse
16 modulus to be half of the axial modulus. The material properties used for the pith and rind for all cases are
17 given in **Table A.1**. The third case (Case (c)) considers both pith and rind as linear elastic isotropic
18 materials, with properties are given in **Table A.1**. In this simulation, we only consider linear elastic
19 behaviors due to a lack of studies regarding multi-axial viscoelastic properties of the tissues.

20 We first simulated uniaxial compression loading to mimic the compression experiment. **Figure A.1**
21 shows the axial force-displacement from the three cases, which indicated that considering an isotropic
22 material model for both rind and pith does not significantly alter the overall force-displacement responses
23 of the stems. From the axial force-displacement responses, the axial stress and strain are constructed to
24 determine the axial properties of the stem. The corresponding contour plots for the axial displacement, axial
25 stress, and axial strain for the three cases are given in **Figure A.2**. From this simulation, we can conclude
26 that when the transverse modulus is stiffer than the axial modulus, the responses are similar to the ones of
27 the isotropic material. In Case (b), the soft lateral modulus leads to more pronounced bulging.

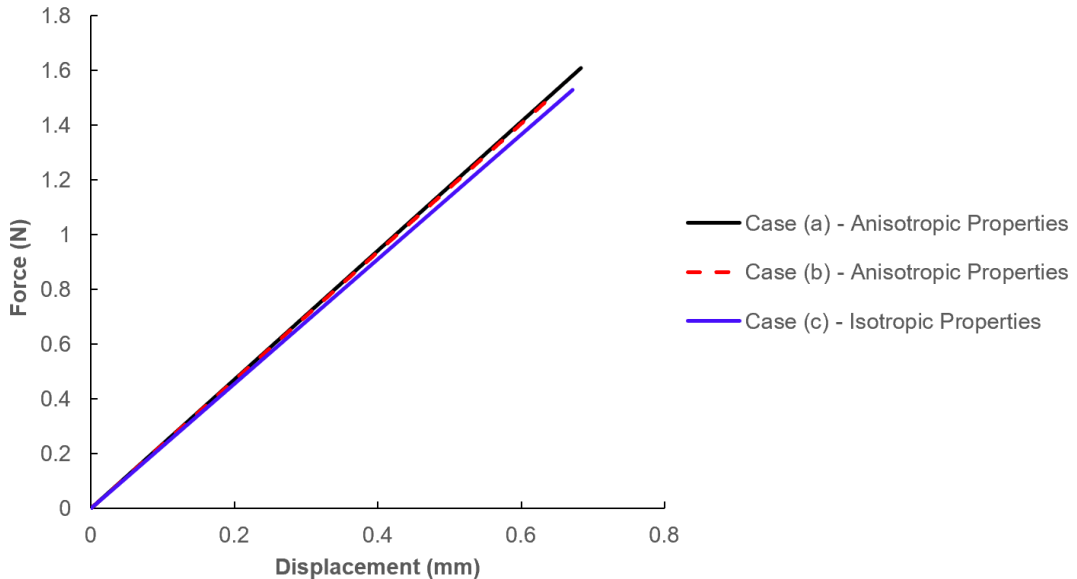
28 We then modeled 4-point bending. **Figure A.3** shows the lateral force-displacement from three
29 cases, which indicated that considering an isotropic material model for pith and rind does not significantly
30 change the overall behavior of the stem. **Figure A.4** also shows the contour plot for the axial displacement,
31 axial stress, and axial strain. Based on this simulation we can see that when the transverse modulus is either
32 softer or stiffer than the axial modulus, the overall responses are comparable to the isotropic material.

1 **Table A.1:** Material properties of pith and rind for isotropic and anisotropic cases

Property	Component	Elastic Modulus (Axial) (MPa)	Elastic Modulus (Transverse) (MPa)	Shear Modulus (Axial) (MPa)	Shear Modulus (Axial) (MPa)	Poisson's Ratio
Isotropic	Rind	325	-	-	-	0.25
	Pith	20	-	-	-	0.25
Anisotropic (case a)	Rind	325	650	130	260	0.25
	Pith	20	40	8	16	0.25
Anisotropic (case b)	Rind	325	162.5	130	65	0.25
	Pith	20	10	8	16	0.25

2

3

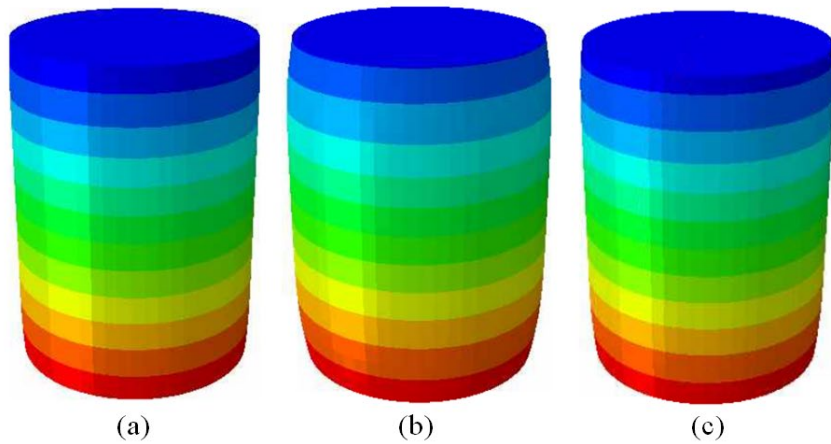
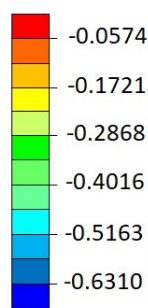


4

5 **Figure A1:** Uniaxial force-displacement from the compression simulations

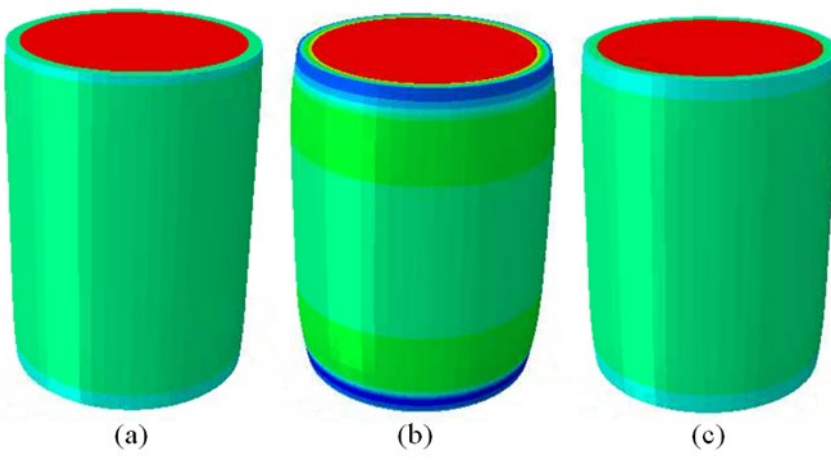
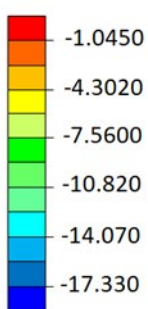
6

1 Axial Displacement



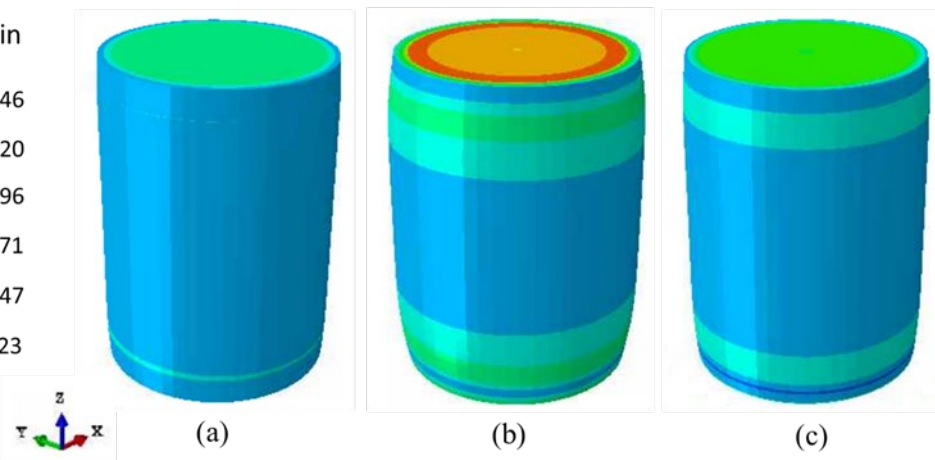
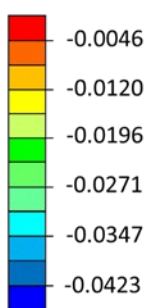
1

2 Axial Stress



2

3 Axial Strain



3

4 **Figure A.2.** Contour plots of axial displacement (in mm), axial stress (in MPa), and axial strain from the
5 three cases

6

7

8

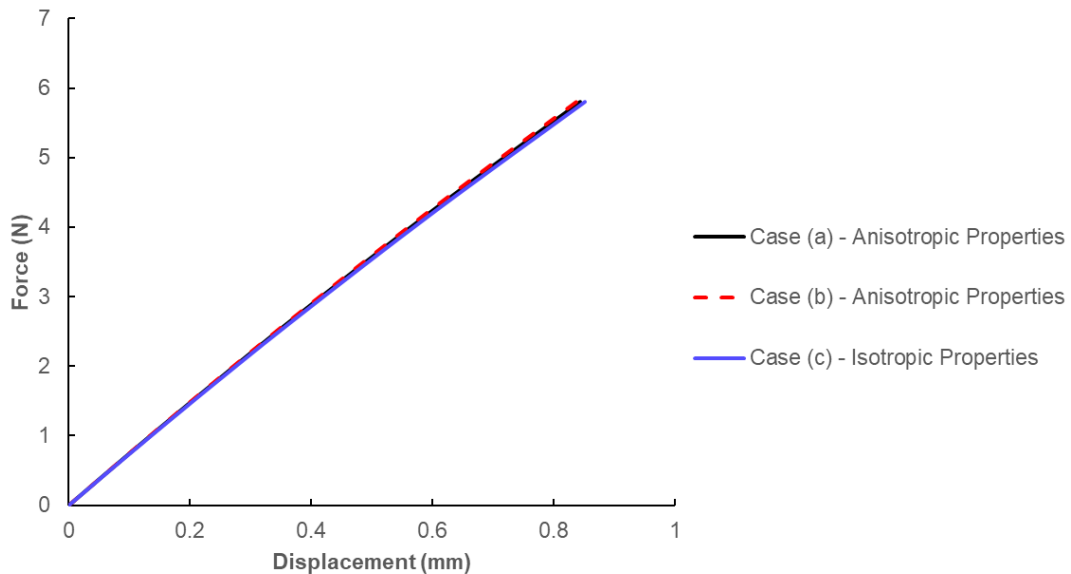
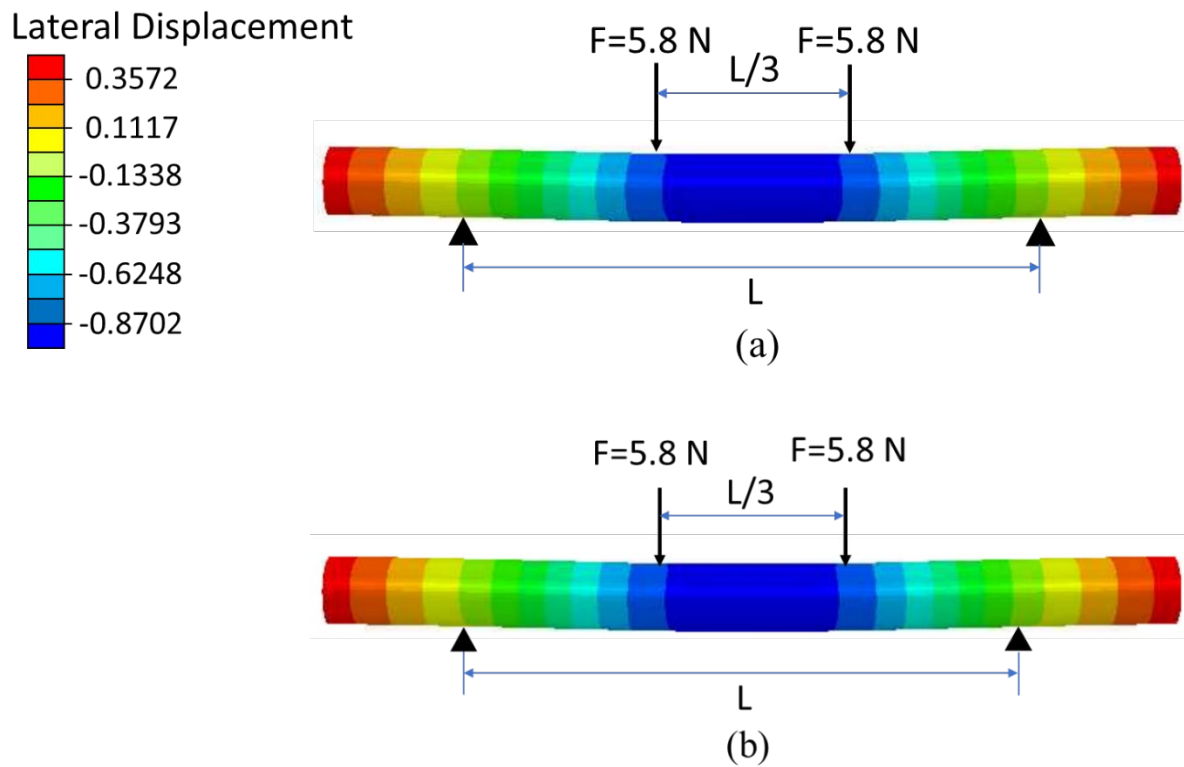
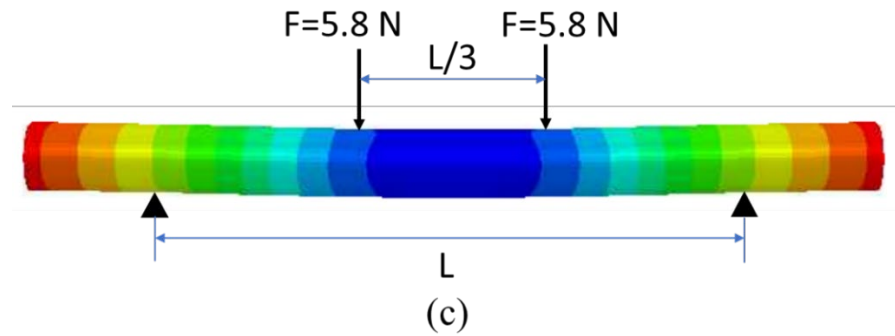
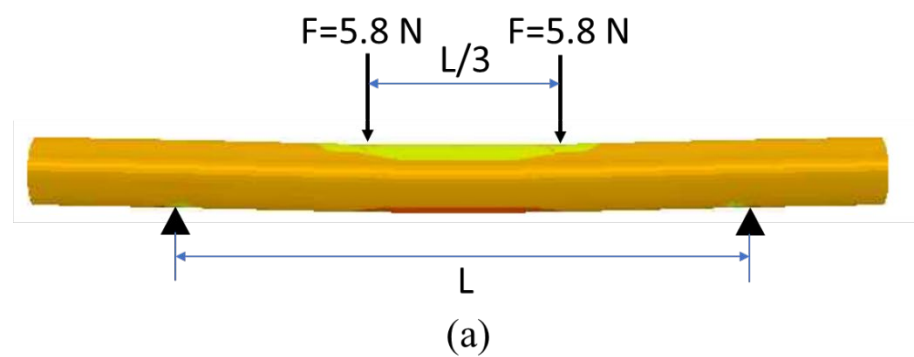
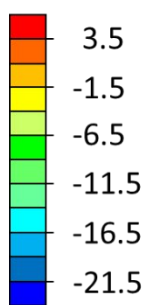


Figure A3: Lateral force-displacement from 4-point bending simulations





Axial Stress

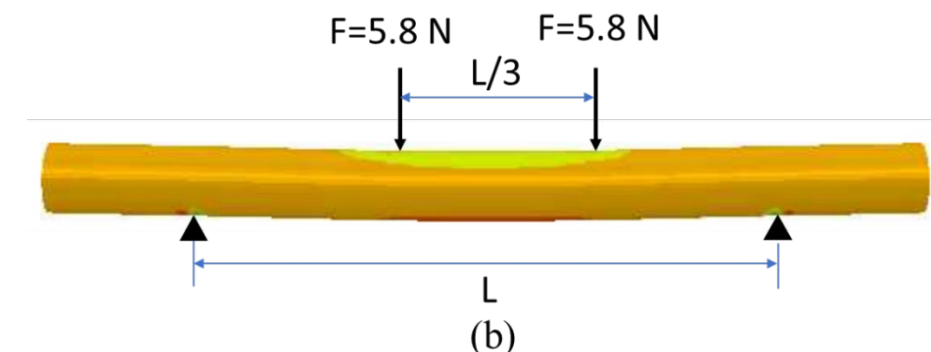


F=5.8 N F=5.8 N

L/3

L

(b)

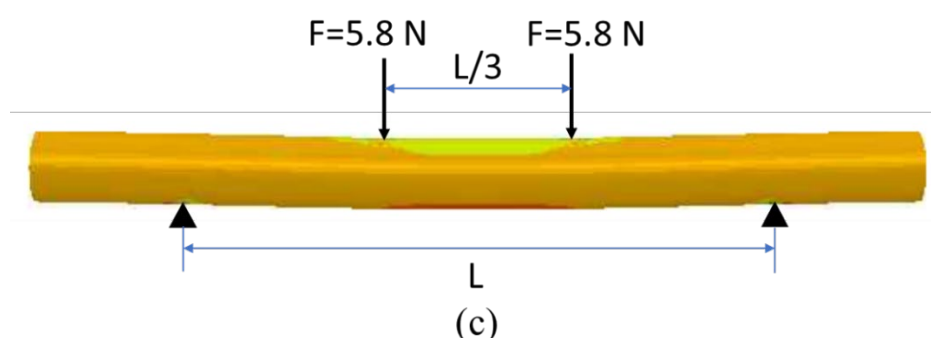


F=5.8 N F=5.8 N

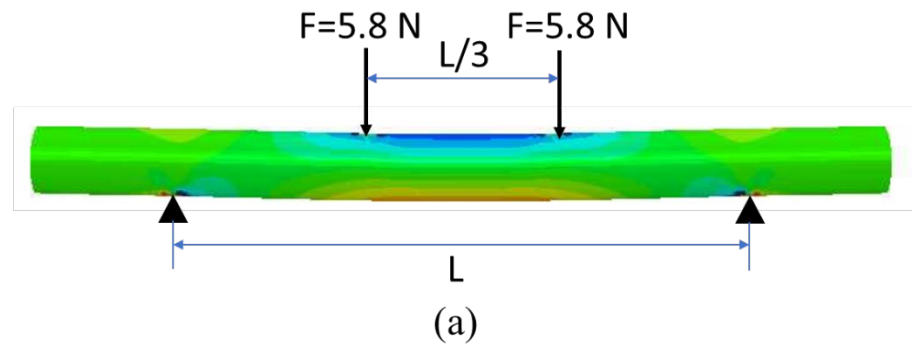
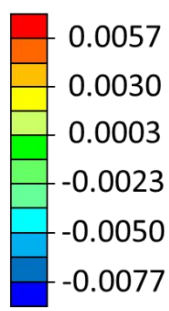
L/3

L

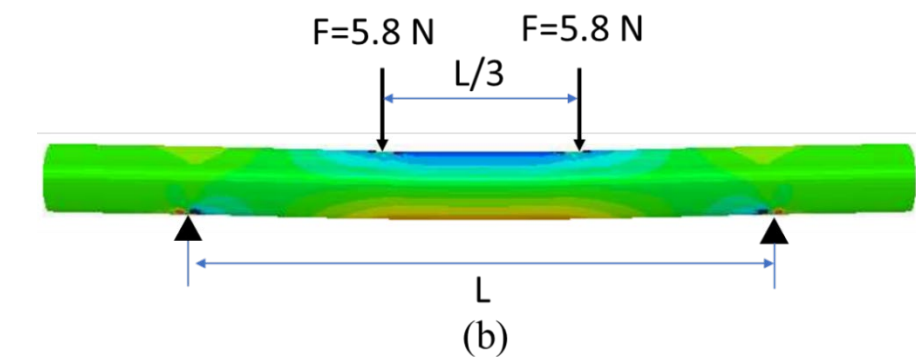
(c)



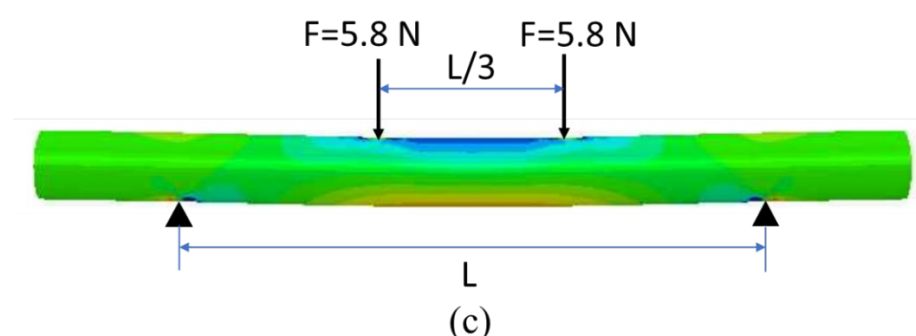
1 Axial Strain



4 (a)



6 (b)



8 (c)

5 **Figure A.4.** Contour plots of lateral displacement (in mm), axial stress (in MPa), and axial strain from the
6 three cases